Naval Research Laboratory
Washington, DC 20375-5320

NRL/MR/6790--09-9230

High Average Current Electron Guns for High-Power FELs

PHILLIP SPRANGLE
JOSEPH PEÑANO

Beam Physics Branch
Plasma Physics Division

BAHMAN HAFIZI

Icarus Research, Inc.
Bethesda, Maryland

DANIEL GORDON
STEVEN GOLD
ANTONIO TING

Beam Physics Branch
Plasma Physics Division

CHAD MITCHELL

NRC Postdoctoral Associate
Washington, D.C.

December 9, 2009

REPORT DOCUMENTATION PAGE

Form Approved
OMB No. 0704-0188

1. REPORT DATE *(DD-MM-YYYY)*	2. REPORT TYPE	3. DATES COVERED *(From - To)*
09-12-2009	Interim	May 2009 – November 2009

4. TITLE AND SUBTITLE

High Average Current Electron Guns for High-Power FELs

5a. CONTRACT NUMBER

5b. GRANT NUMBER

5c. PROGRAM ELEMENT NUMBER
67-9252-00

6. AUTHOR(S)

Phillip Sprangle, Joseph Peñano, Bahman Hafizi,* Daniel Gordon, Steven Gold, Antonio Ting, and Chad Mitchell†

5d. PROJECT NUMBER

5e. TASK NUMBER

5f. WORK UNIT NUMBER

7. PERFORMING ORGANIZATION NAME(S) AND ADDRESS(ES)

Naval Research Laboratory
4555 Overlook Avenue, SW
Washington, DC 20375-5320

8. PERFORMING ORGANIZATION REPORT NUMBER

NRL/MR/6790--09-9230

9. SPONSORING / MONITORING AGENCY NAME(S) AND ADDRESS(ES)

Office of Naval Research
One Liberty Center
875 North Randolph St.
Arlington, VA 22203-1995

10. SPONSOR / MONITOR'S ACRONYM(S)

ONR

11. SPONSOR / MONITOR'S REPORT NUMBER(S)

12. DISTRIBUTION / AVAILABILITY STATEMENT

Approved for public release; distribution is unlimited.

13. SUPPLEMENTARY NOTES

*Icarus Research, Inc., P.O. Box 30780, Bethesda, MD 20814-0780
†NRC Postdoctoral Associate, Washington, DC 20001

14. ABSTRACT

High average power FELs require high average current electron injectors capable of generating high quality, short duration electron bunches with a repetition rate equal to the frequency of the rf linac. In this paper, we propose, analyze and simulate an rf-gated, gridded thermionic electron gun for use in high average power FELs. In the proposed configuration, the rf-gated grid is modulated at the fundamental and 3rd harmonic of the linac frequency. The addition of the 3rd harmonic on the grid results in shorter electron bunches. In this configuration, every rf bucket of the linac accelerating field contains an electron bunch. PIC simulations indicate that this approach can provide the necessary charge per bunch, bunch duration, longitudinal and transverse emittance, and repetition rate for high average power FELs operating in the IR regime.

15. SUBJECT TERMS

High-power FEL
High average current injector
RF-gated thermonic gun

16. SECURITY CLASSIFICATION OF:			17. LIMITATION OF ABSTRACT	18. NUMBER OF PAGES	19a. NAME OF RESPONSIBLE PERSON
a. REPORT	b. ABSTRACT	c. THIS PAGE			Phillip Sprangle
Unclassified	Unclassified	Unclassified	UL	40	19b. TELEPHONE NUMBER *(include area code)* (202) 767-3493

Standard Form 298 (Rev. 8-98)
Prescribed by ANSI Std. Z39.18

Table of Contents

High Average Current Electron Guns for High-Power FELs

Phillip Sprangle, Joseph Peñano, Bahman Hafizi[1], Daniel Gordon

Steven Gold, Antonio Ting and Chad Mitchell[2]

Plasma Physics Division
Naval Research Laboratory
Washington DC

Abstract

High average power FELs require high average current electron injectors capable of generating high quality, short duration electron bunches with a repetition rate equal to the frequency of the rf linac. In this paper we propose, analyze and simulate an rf-gated, gridded thermionic electron gun for use in high average power FELs. Thermionic cathodes can provide the necessary high current, have long life times and require modest vacuums. In the proposed configuration the rf-gated grid is modulated at the fundamental and 3rd harmonic of the linac frequency. The addition of the 3rd harmonic on the grid results in shorter electron bunches. In this configuration, every rf bucket of the linac accelerating field contains an electron bunch. PIC simulations indicate that this approach can provide the necessary charge per bunch, bunch duration, longitudinal and transverse emittance, and repetition rate for high average power FELs operating in the IR regime.

1. Icarus Research, Inc

2. National Research Council Postdoctoral Fellow

I. Introduction

High average power free electron lasers (FELs) require a train of short duration, high repetition rate and high peak current electron bunches having high quality and high average current [1]. These requirements place stringent constraints on the electron gun [2-4].

Figure 1 shows a schematic of an FEL injector for high average power operation. For IR FELs the typical electron beam parameters associated with the various stages in the injector are indicated. The injector should produce an electron pulse train with short (~ 10 psec rms) bunches at a repetition frequency of ~ 700 MHz, with energies of ~ 5-8 MeV, charge per bunch of ~ 1 nC, normalized transverse emittance of $\varepsilon_n < 15\,\text{mm} - \text{mrad}$, and a bunch radius of $R_b < 0.5\,\text{mm}$. Before entering the FEL wiggler the electron bunches are accelerated in an energy recovery linac (ERL) to ~ 80 MeV with a fractional energy spread $\Delta E/E < 0.5\%$, peak bunch current $I_b > 300\,\text{A}$ and an average current of ~1 A, while preserving the beam emittance and radius. Here the charge per bunch is $q N_b = I_b \tau_b \sim 1\,\text{nC}$ and the bunch duration entering the wiggler is $\tau_b \sim 5\,\text{psec}$. The beam quality requirements for high-power IR FEL operation are discussed in more detail in Appendix A. In addition, high average power FELs [5-8] require high wall-plug efficiencies [9].

Photocathode guns are capable of generating short, high-quality and high-charge electron bunches and are employed in the majority of FELs [1-4,10-13]. However, thermal issues, short lifetimes and drive-laser average-power requirements currently present limitations when operated at high-average powers.

Thermionic guns (Appendix B) have demonstrated long life-time operation and high average currents. Several FELs have used thermionic guns such as the Boeing [14], the Stanford U. [15,16], the Novosibirsk [17], and the SPring-8 [18,19] FELs. These guns cannot be used for high average power IR FELs because of their low repetition rate which was limited because the grids were not directly driven with rf. Here, we propose a new injector configuration based on a thermionic gun that can satisfy all of the requirements for a high-average power IR FEL.

This paper proposes the use of rf-gated, harmonically driven, gridded thermionic electron guns for MW-class IR FELs. In the proposed configuration, the rf-gated grid is modulated at the fundamental and 3rd harmonic of the rf linac frequency, e.g., ~ 700 MHz and ~ 2.1 GHz. Simulations indicate that the required electron beam quality, pulse duration and average current for MW-class FEL operation can be achieved with this configuration. In addition, the heat radiated by the thermionic gun in the proposed design is relatively small, and hence it can be used with either a normal-conducting NCRF or superconducting SRF pre-booster RF cavities [3,4,10].

In Section II we discuss the characteristics of the rf-gated, gridded thermionic gun and the use of rf harmonics to generate short electron bunches. Section II also contains an analysis and estimates of the bunch emittance due to the grid. Section III presents the results of PIC simulations using TurboWAVE. Section IV summarizes our theoretical and numerical results.

II. RF-Gated, Gridded Thermionic Gun

Figure 2 shows a schematic of the rf gated, gridded thermionic cathode configuration. The grid consists of an array of concentric wires, close to the cathode, that is modulated by rf fields. The grid has a negative DC bias with respect to the cathode, in addition to the rf fields at the fundamental and 3rd harmonic of the linac frequency. Since the grid is modulated at the fundamental linac frequency, every accelerating rf bucket is filled. The addition of the 3rd harmonic provides shorter electron bunches. The typical parameters of the gun are shown in Table I. The key characteristics of the gun are discussed below.

a) Thermionic Cathode

Thermionic cathodes can provide the necessary high average current for high average power FELs [14-21]. They operate at moderate vacuums ($10^{-8} - 10^{-7}$ Torr) and can have long lifetimes (> 10,000 hours) delivering over 10^8 Coulombs. As an example, for a cathode current density of $J = 10\,\mathrm{A/cm^2}$, the charge per bunch is $q N_b = \pi R_b^2 J \tau_b \approx 1\,\mathrm{nC}$ for a bunch radius $R_b = 0.5\,\mathrm{cm}$ and bunch duration $\tau_b = 150\,\mathrm{psec\,(rms)}$. These parameters are readily achieved with conventional thermionic

cathodes. One candidate for this application is a dispenser cathode which can generate current densities of ~ 20 A/cm^2, while more advanced cathodes (with controlled porosity) can generate up to ~ 100 A/cm^2. Single crystal cathodes such as lanthanum hexaboride and cerium hexaboride are robust and can generate up to ~ 100 A/cm^2, but require high temperature [18,19]. Dispenser cathodes employing scandate oxides have low work functions (~ 1.5 eV), high current densities (> 100 A/cm^2) and long lifetimes (>1000 hr.), but may have poor reproducibility and non-uniform emission [20].

The current-voltage characteristics of thermionic cathodes are determined by the material, temperature as well as the external and space-charge fields. In the steady-state, 1-D limit, the space-charge limited current density is given by the Child-Langmuir relationship [20,22-24], $J_{CL}[\mathrm{A/cm^2}] = 2.33\times10^{-6}\,\Phi^{3/2}[\mathrm{V}]/d^2[\mathrm{cm}]$, where $\Phi \geq 0$ is the voltage difference between the two conducting planes and d is the separation.

In the temperature-limited regime, i.e., the Richardson-Dushman-Schottky limit, the current density is given by [25,26]:
$J_{RDS}[\mathrm{A/cm^2}] = A_o T_c^2 \exp\{-11605\,\Phi_{WF}/T_c\}\exp\{4.4(\Phi[\mathrm{V}]/d[\mathrm{cm}])^{1/2}/T_c\}$, where $A_o = 120\,\mathrm{A/(cm^2-K^2)}$, Φ_{WF} is the work function (eV) of the cathode and T_c is the temperature (K). The above value for A_o is the theoretically derived value while the experimentally-measured value for CeB_6 indicates that $A_o \approx 20\,\mathrm{A/(cm^2-K^2)}$ [18].

The Child-Langmuir and the Richardson-Dushman-Schottky regimes are plotted in Fig. 3 for $d = 250\,\mu\mathrm{m}$, $\Phi_{WF} = 1.9\,\mathrm{eV}$, $T_c = 1300\,\mathrm{K}$ and $A_o = 120\,\mathrm{A/(cm^2-K^2)}$. The optimum operating regime for the rf-gated gun is near the intersection of the space-charge and thermal limits where the current density is not sensitive to fluctuations in the cathode temperature as shown in Fig. 3.

There is a third emission regime in which a high surface electric field $E_S \sim 10^7 - 10^8$ V/cm is employed to extract electrons by tunneling. This field emission regime is particularly effective when the cathode consists of sharp tips. In this regime the current density is given by the Fowler-Nordheim relation [20,27],

$J_{FN}\,[\mathrm{A/cm^2}] = A_{FN}\,E_S^2 \exp(-B_{FN}/E_S + 9.8/\sqrt{\Phi_{WF}})$, where $A_{FN}[\mathrm{A/V^2}] \approx 1.4\times10^{-6}/\Phi_{WF}$, $B_{FN}[\mathrm{V/cm}] \approx 6.5\times10^{7}\,\Phi_{WF}^{3/2}$ and E_S is in units of V/cm. Field emitting cathodes are also being considered for high average current guns for FELs [28].

b) RF-Gated Grid

The actual grid configuration consists of a series of concentric rings and radial spokes located close to the cathode surface as shown in Fig. 2. However, for the purpose of the following analysis, the rings are modeled by an array of parallel wires as shown in Fig. 4 and the rf modulation is treated electro-statically.

The potential on the grid wires is Φ_G, the potential difference between the cathode and anode is Φ_A and the electric field is $-\Phi_A/z_A$. The grid wires are parallel to the y-axis, separated by a distance $2a$ and located at $z=z_G$. The radius of the grid wires is taken to be small, $r_o \ll a,\ z_G$. The potential in the cathode-grid-anode region is given by [Appendix C]

$$\Phi(x,z) = -\sum_{n=\pm1,\pm3,..}\left[\Phi_O \ln\frac{G_n(x,z)}{F_n(x,z)} + \Phi_A\frac{r_o^2\,(z-z_G)/z_A}{G_n(x,z)}\right] + \Phi_A\frac{z}{z_A}, \qquad (1)$$

where $\Phi_O = (1/2)\left(\Phi_G - \Phi_A\, z_G/z_A\right)\left(\ln(2\,z_G/r_o) + M_o\right)^{-1}$, $F_n(x,z)=(x-n\,a)^2+(z+z_G)^2$, $G_n(x,z)=(x-n\,a)^2+(z-z_G)^2$, $M_o = \sum_{l=1,2,3.}^{\infty}\ln\left(1 + z_G^2/(\ell^2\,a^2)\right)$ and the sum is over the grid wires. The first term in the sum represents the potential due to the grid wires and their images from the cathode. The second term is a contribution induced by the electric field between the anode and cathode and is localized to the region around the wires. The last term in Eq.(1) represents the cathode-anode gap potential. The potential satisfies the appropriate boundary conditions on the cathode, grid and anode surfaces.

The grid potential is the sum of a constant (DC) and a time varying (RF) contribution, i.e., $\Phi_G(t) = \Phi_{DC} + \Phi_{RF}(t)$. The rf grid potential is given by

$$\Phi_{RF}(t) = \Phi_1\cos(\omega_{RF}t + \varphi_1) + \Phi_3\cos(3\,\omega_{RF}t + \varphi_3),$$

where ω_{RF} is the fundamental linac frequency, Φ_ℓ is the amplitude of the ℓ^{th} harmonic, φ_ℓ is a constant phase and $\ell = 1$ or 3. For parameters of interest the electrostatic

approximation is valid, in the absence of beam loading effects, since the electron transit time $\tau_{transit} \sim z_G / v_z \sim 30\,\text{psec}$ between the cathode and grid is small compared to the rf period, $\tau_{RF} = 2\pi / \omega_{RF} \sim 1.4\,\text{nsec}$.

Figure 5 illustrates the grid potential modulation that can be achieved using DC bias, fundamental and 3rd harmonic. The figure schematically indicates the generation of short electron bunches of ~ 100 psec (rms) duration can be obtained at a repetition rate of 700 MHz. Shorter bunches can be achieved by the addition of higher harmonics, e.g., 5th harmonic at 3.5 GHz.

Electron emission takes place when the axial electric field on the cathode surface is negative. The axial field on the cathode (in the absence of space charge), from Eq.(C5) in Appendix C, is

$$E_z(x, z=0) = -\Phi_A / z_A - \mu(x)(\Phi_G / z_G - \Phi_A / z_A), \qquad (2)$$

where $0 < \mu(x) < 1$ is a shielding parameter defined in Eq.(C6). The shielding parameter represents the reduction of the anode field due to the presence of the grid wires. The shielding of the electric field on the cathode is minimum between the wires and maximum beneath the wires. Typically for our parameters, $0.7 < \mu(x) < 0.9$. The shielding parameter controls electron emission and current density from the cathode. Figure 6 shows a plot of $\mu(x)$ and axial electric field $E_z(x, z=0)$ on the cathode, extending over a region covering three grid wires for $t = \pi / \omega_{RF}$. It should be noted that a small variation in $\mu(x)$ is sufficient to cause a relatively large change in E_z and electron flux across the surface.

c) Bunch Emittance

There are several sources that contribute to the emittance of the electron bunch [22,23,29]. The contribution to the normalized emittance from the finite cathode temperature is $\varepsilon_{n,T} = (1/2) R_c (k_B T_c / mc^2)^{1/2} \approx 1.2\,\text{mm-mrad}$, where $T_c = 1300\,K$ is the cathode temperature and $R_c = 0.5\,\text{cm}$ is the cathode radius. The emittance contribution due to a magnetic field on the cathode is $\varepsilon_{n,B} = q B_o R_c^2 / 2mc^2 \approx 0.7\,\text{mm-mrad}$, where $B_o = 1\text{G}$ is the assumed magnetic field on the cathode from the Earth and other stray sources, and $R_c = 0.5\,\text{cm}$. Roughness on the

cathode contributes to the emittance by an amount on the order of $\varepsilon_{n,R} = \pi h/(2\ell) R_c (q E_S h/2mc^2)^{1/2} \sim 0.7\,\text{mm}-\text{mrad}$, where $h = 1\,\mu\text{m}$ is the amplitude of surface roughness, $\ell = 20\,\mu\text{m}$ is the period of the roughness, $E_S = 5\,\text{MV/m}$ is the surface field and $R_c = 0.5\,\text{cm}$.

The emittance due to a single grid wire, as shown in Fig. 7, in the absence of self fields, is given by (Appendix C)

$$\varepsilon_{n,grid} \approx R_b \langle \beta_x \rangle \approx \frac{2\mu_1(a)}{3}\left(\frac{a}{z_G}\right) R_b \frac{\left|\overline{\Phi}_G - (z_G/z_A)\overline{\Phi}_A\right|}{(z_G/z_A)^{1/2}\,\overline{\Phi}_A^{1/2}}, \qquad (3)$$

where $R_b \approx R_c$ is the beam radius, $\langle \beta_x \rangle$ is the averaged normalized electron velocity, $\mu_1(a)$ is the shielding parameter due to one wire (Appendix C), $\overline{\Phi}_G = |q|\Phi_G/(mc^2)$ and $\overline{\Phi}_A = |q|\Phi_A/(mc^2)$. Using typical values for the gun parameters, the normalized emittance due to the grid is $\varepsilon_{n,grid}\,[\text{mm}-\text{mrad}] \sim 5-10\,R_b[\text{cm}]$. This range of emittances is consistent with PIC simulation results which are presented in the next section.

III. PIC Simulations

To simulate more realistic geometries in the gun configuration and include spacc charge effects, the PIC code TurboWAVE [30] is used. TurboWAVE is a 2 or 3-D, fully-relativistic PIC code that modcls a variety of physical processes. Here we describe two-dimensional slab and axially symmetric electrostatic simulations of the gun. In these simulations the cathode and anode are held at fixed potentials, while the grid consists of parallel wires or concentric rings whose potential is a prescribed function of time. The potential at all other locations within the gun region is computed via successive over-relaxation, and includes space charge effects.

Figure 8 shows an illustration of the electron dynamics including space charge effects in the cathode-grid region. In this simulation an infinite array of parallel wires using a 2-D slab geometry was employed. The grid potential is $\Phi_G(t) = -360 - 38\cos(\omega_{RF} t) + 36\cos(2\omega_{RF} t) - 33\cos(3\omega_{RF} t)$ in units of volts and the fundamental frequency is $f_{RF} = \omega_{RF}/2\pi = 700\,\text{MHz}$. The cathode-anode gap is $z_A = 1\,\text{cm}$ and the cathode – anode potential is 50 kV. The grid wire radius is

$r_o = 30\,\mu\,\mathrm{m}$. A constant electron density is maintained on the cathode and the electrons are emitted and propagated by the external and space charge fields. The time-integrated current density is shown in Fig.8 along with potential contours at the peak of emission. Only three spatial periods of the infinite grid structure are shown in the figure. The particles are primarily emitted between the wires so that the grid current (grid heating) is very low. This is due to the shielding effect of the grid wires on the electric field, as discussed in Appendix C. The shielding parameter for the parameters of Fig.8 is $\mu = 0.8$ between the wires and $\mu = 0.87$ beneath the wires.

As another example, TurboWAVE is used in cylindrical geometry to simulate the ring grid configuration shown in Fig. 9. The configuration of the gun shown in Fig. 9 includes focusing electrodes, at 45 degrees, which are found to reduce the emittance. The current pulses produced at the grid plane and the anode plane are shown in Fig. 10, along with the time varying potential of the grid wires. In this example, 60 psec (rms) bunches having a charge of 0.7 nC are generated. The average current is $\langle I_b \rangle = 0.5\,\mathrm{A}$. Figure 11 shows the slice emittance, which at the peak of the current pulse is ~ 5 mm-mrad. The projected transverse phase space, shown in Fig. 12, corresponds to a projected emittance of $\varepsilon_n = 8.9\,\mathrm{mm-mrad}$. This is also shown as the horizontal dashed line in Fig. 11. The longitudinal phase space shown in Fig. 13 is characterized by a longitudinal emittance of $\varepsilon_z = 20\,\mathrm{keV\text{-}psec}$.

TurboWAVE has also been used to determine the effect of beam loading in the cathode-grid region. A simple estimate indicates that beam loading is not important for the parameters under consideration. The rf fill time, i.e., the time it takes to fill the cathode-grid region with rf energy, is $\tau_F \approx R_c / c \sim 30\,\mathrm{psec}$, which is short compared to the rf period, $\tau_{RF} \approx 1.4\,\mathrm{nsec}$. In addition, for the parameters being considered the ratio of the kinetic energy of the electron bunch crossing the grid plane to the rf energy in the cathode-grid region is $W_b / W_{RF} < 1$, where $W_b \sim q N_b \Phi_G$, $W_{RF} = (2/15)(R_c^2/(z_G r_e))(q\Phi_G / mc^2) q\Phi_G$ and $r_e = q^2 / mc^2$. Since $W_b / W_{RF} < 1$ and the electron bunch duration at the grid plane $\tau_b \sim 100$ psec is greater than τ_F, the rf energy in the cathode-grid region is not significantly depleted by the electron bunch.

Simulations using TurboWAVE are consistent with the above arguments that beam loading for the parameters under consideration is not significant.

IV. Conclusion

In this paper we have proposed, analyzed and simulated an rf-gated, gridded thermionic gun for high average power IR FELs. Simulations using TurboWAVE indicate that the necessary electron beam parameters for the FEL, i.e., charge per bunch, average current, quality and pulse format, can be achieved. The beam emittance induced by the grid is within acceptable limits for operation in the IR regime. There are a number of techniques for further reducing bunch emittance, including anode shaping, grid shadowing and emittance compensation coils. The required high average current can be obtained with dispenser or single-crystal thermionic cathodes which are robust and have long lifetimes. Thermionic cathodes can provide the necessary high average current, charge per bunch and pulse format for high average power FELs. They operate at moderate vacuums ($10^{-8} - 10^{-7}$ Torr), have long lifetimes (> 10,000 hours) delivering over 10^8 Coulombs and can provide cathode current densities $> 10\,A/cm^2$. The pulse duration requirements can be met by modulating the grid with a combination of the fundamental and 3rd harmonic of the linac frequency, filling every rf bucket in the linac. The heat radiated by the thermionic gun in the proposed designed is relatively small and hence it can be configured with either normal-conducting NCRF or super-conducting SRF pre-booster cavities. An experimental program is under way at the Naval Research Laboratory to demonstrate this high average current electron gun configuration.

Acknowledgements: The authors are grateful to Professor P. Serafim for useful discussions. This work was supported by the Office of Naval Research.

Appendix A: Electron Beam Quality Requirements for FELs

In the FEL, the gain, growth rate and efficiency are sensitively dependent on the axial velocity spread $\Delta\beta_z$ of the electrons. The electron beam quality is measured in terms of emittance and energy spread, the origins of which include i) temperature of the cathode, ii) roughness of the emitting surface, iii) uniformity of the emission from the cathode surface, iv) uniformity of electric and magnetic fields, and v) self-fields. In addition, the FEL gain/growth rate depends on the current from the gun, or rather on the peak current produced after bunching in the injector and accelerator. The axial velocity spread can be expressed in terms of energy spread, transverse emittance and bunch radius. The electron bunch quality requirement for the FEL $\Delta\beta_z << \lambda / 2L_{eff}$ can be expressed by the following inequality [31]

$$\Delta E_{total} / E = \Delta E / E + \varepsilon_{n,\perp}^2 / (2R_b^2) + \pi^2 a_w^2 R_b^2 / (2\lambda_w^2) < \lambda_w (1 + a_w^2 / 2) / (4 L_{eff}). \quad \text{(A1)}$$

In this expression, the first term represents the fractional intrinsic energy spread, the second term arises from the transverse emittance $\varepsilon_{n,\perp}$, and the third term is due to transverse wiggler gradients. The right hand side of this expression is the FEL conversion efficiency, where L_{eff} is the gain length in the case of the amplifier or the wiggler length in the case of the oscillator, a_w is the wiggler parameter and λ_w is the wiggler period. The fractional energy spread can be written in terms of the normalized longitudinal emittance ε_z,

$$\frac{\Delta E}{E} = \frac{\varepsilon_z}{\tau_b E} = \frac{\varepsilon_z^*}{m L_b E}, \quad \text{(A2)}$$

where $\varepsilon_z^* = mc\varepsilon_z$, L_b is the electron pulse length and τ_b is the pulse duration. When the inequality in Eq.(A1) is satisfied the spread in the axial velocity of the electrons is sufficiently small for the FEL to lase. Independent of other considerations, the three contributions to the velocity spread in Eq.(A1) should be approximately equal. For the MW-class FEL operating in the IR the required parameters are $\varepsilon_{n,\perp} < 20\,\text{mm} - \text{mrad}$, $\varepsilon_z < 200$ keV − psec, $R_b < 0.5\,\text{mm}$, $\tau_b < 3\,\text{psec}$, for a peak electron bunch current of ~ 500 A. For these parameters $\Delta E / E \leq 5\%$.

Appendix B: Thermionic Injectors

The gridded electron guns used as injectors for rf linacs in several notable FEL experiments, including the Stanford, Boeing, and Novosibirsk FEL injectors, have operated at subharmonics of the main linac frequency, and have used short high voltage pulses synchronized to the phase of the rf to gate the emission and generate electron bunches suitable for injection into the subharmonic cavities. The original Stanford FEL gun [16] was the first to use this approach, producing 200 pC, 1.3 ns electron bunches at 11.8 MHz at the entrance of the normally conducting injector section of a 1.3 GHz superconducting linac.

Operating at the 12^{th} subharmonic accomplished two critical goals. First, it permitted the use of a relatively long high voltage pulse to drive the grid of the electron gun; operating the first rf cavity at 1300 MHz while filling the same fraction of an rf period would have required the generation of a 170 psec drive pulse as well as an rf gun capable of modulating the current on that time scale. Second, it allowed the use of subharmonic bunching to increase the peak current to the level required for the FEL.

However, the problem with subharmonic bunching is that while increasing peak current, it ultimately limits the average current, since it limits the fraction of rf buckets that are filled with electrons, while the charge in each bucket is limited by space-charge effects. Using a similar approach, the non-superconducting Energy Recovery Linac FEL in Novosibirsk [17] used a 300 keV electron gun with ~1 A of peak current in a 1.5 ns pulse at a maximum repetition rate of 22.5 MHz (eighth subharmonic of the ~180 MHz linac). In this case, the maximum average current was 20 mA.

The SPring-8 FEL adopted an innovative approach to producing a high brightness, bunched beam from a thermionic cathode without using a control grid [18,19]. The experiment employs a single-crystal CeB_6 cathode to produce a high current density 500-keV beam from an electron gun driven by a high-voltage modulator. At the exit to the gun, a beam with a 1 A peak current and 3 μs pulse width at a maximum repetition rate of 60 Hz was generated. A single nanosecond bunch is then generated from each pulse by means of a beam chopper. Thus, more than 99.9% of the beam is deposited in a beam dump. This gridless approach thus solves the problem of producing

a clean, low-emittance electron bunch, but at the cost of depositing most of the beam current in a beam dump, an approach that is inconsistent with high average current applications.

A high average current injector should aim to fill every rf bucket. For a 700 MHz linac with no subharmonic section, a thermionic injector must generate electron bunches of order 100 psec in pulse length at a 700 MHz pulse repetition rate. Moreover, in order to produce an average current of ~1 A, the instantaneous current should be about an order of magnitude higher. For such short bunches and high repetition rate, it is not practical to generate short high voltage pulses to apply to the grid of an electron gun, and direct rf modulation of the grid is required.

Gridded electron guns are used in Inductive Output Tube (IOT) amplifiers [32-34] and can generate average currents of ~1 A, peak currents of ~ 5–10 A, cathode-anode voltages of ~ 35 kV, and modulation frequencies > 1 GHz. These guns use low-temperature dispenser cathodes combined with grids fabricated from pyrolytic graphite, a polycrystalline form of carbon that will operate at high temperatures and has improved strength and uniformity compared to grids made of tungsten or molybdenum [34]. The grid is typically placed within ~100–300 μm of the cathode to permit high-frequency current modulation. In typical operation, these guns are employed to produce electron bunches filling 180° of rf phase in order to generate the maximum rf power at the drive frequency. However, the degree of beam modulation is not constrained to be 180° of the rf phase; it depends on the negative bias voltage between the grid and the cathode (typically of order 100–200 V) as well as the rf voltage induced in the cathode-grid gap. Shorter bunches can in principle be obtained by driving the grid circuit simultaneously at the fundamental rf frequency and a higher harmonic.

Appendix C: Grid Fields and Beam Emittance

For the purpose of estimating the electron beam emittance due to a grid, we consider the 2D cathode, grid, anode configuration shown in Fig. 4. The grid wires form an infinite array located at $z = z_G$, are parallel to the y-axis and are separated by a distance $2a$. The radius of the grid wires is small, $r_o << a,\ z_G$. The grounded cathode is located at $z = 0$ and the anode at $z = z_A$. The potential on the grid relative to the cathode is denoted by $\Phi_G(t)$ and consists of a dc bias and rf component while the anode potential is $\Phi_A(t)$. In addition, the field in the anode-cathode gap induces a dipole field around each grid wire. The dipole field is localized around the grid wire and has little effect on the electron motion. Although the grid voltage varies at the rf frequency, it can be considered to be constant for the purpose of this calculation since the electron transit time from the cathode to the grid, $\tau_G = z_G / v_z \sim 0.1\,\text{nsec}$, is small compared to the rf period, $\tau_{RF} \sim 1.4\,\text{nsec}$.

a) Potential for an Array of Grid Wires

The potential associated with a single grid wire located at $x = 0$ and $z = z_G$ (see Fig. 4), is

$$\Phi(x,z) = -\Phi_O \ln\left(\frac{x^2 + (z-z_G)^2}{x^2 + (z+z_G)^2}\right) + \Phi_A \frac{z}{z_A} - \Phi_A \frac{(z-z_G)}{z_A}\left(\frac{r_o^2}{x^2 + (z-z_G)^2}\right), \qquad \text{(C1)}$$

where $\Phi_O = (1/2)(\Phi_G(t) - \Phi_A(t)(z_G / z_A)) / \ln(2\,z_G / r_o)$. In Eq.(C1) the first term is the potential of a line charge together with its image due to the cathode, the second term is due to the anode potential and the third term is due to the induced dipole charges on the wire. For $r_o << a,\ z_G$ the potential on the cathode is zero, on the surface of the grid wire it is $\Phi_G(t)$ and on the anode it is $\Phi_A(t)$. For the typical parameters considered here $|\Phi_G| \approx 100\,\text{V}, \Phi_A \approx 40\,\text{kV}$, $z_G \approx 250\,\mu\text{m}$, $z_A \approx 1\,\text{cm}$, $a \approx 200\,\mu\text{m}$, $r_o \approx 30\,\mu\text{m}$ and $\ln(2\,z_G / r_o) \sim 3$.

The fields associated with the single grid wire potential, $\mathbf{E} = -\nabla\Phi$, are

$$E_x = -2\Phi_O\left(\frac{x}{x^2+(z+z_G)^2} - \frac{x}{x^2+(z-z_G)^2}\right) - 2\frac{\Phi_A r_o^2}{z_A}\left(\frac{(z-z_G)x}{(x^2+(z-z_G)^2)^2}\right), \qquad \text{(C2a)}$$

$$E_z = -2\Phi_o\left(\frac{(z+z_G)}{x^2+(z+z_G)^2}-\frac{(z-z_G)}{x^2+(z-z_G)^2}\right)-\frac{\Phi_A}{z_A}+\frac{\Phi_A r_o^2}{z_A}\left(\frac{x^2-(z-z_G)^2}{(x^2+(z-z_G)^2)^2}\right). \quad \text{(C2b)}$$

The dipole contribution, last term in Eqns. (C2), is small and can be neglected near the cathode for $z_G >> r_o$.

The potential due to an infinite array of grid wires, centered at $z = z_G$ and $x = \pm a, \pm 3a, \pm 5a, \ldots$, is given by

$$\Phi(x,z) = -\sum_{n=\pm 1,\pm 3,}\left[\Phi_o \ln\frac{G_n(x,z)}{F_n(x,z)} + \Phi_A \frac{r_o^2 (z-z_G)/z_A}{G_n(x,z)}\right] + \Phi_A \frac{z}{z_A}, \quad \text{(C3)}$$

where $\Phi_o = (1/2)(\Phi_G - \Phi_A z_G / z_A)(\ln(2 z_G / r_o) + M_o)^{-1}$,

$F_n(x,z) = (x - na)^2 + (z + z_G)^2$, $G_n(x,z) = (x - na)^2 + (z - z_G)^2$ and

$M_o = \sum_{l=1,2,3,}^{\infty} \ln\left(1 + z_G^2/(\ell^2 a^2)\right)$. The corresponding electric field in the cathode-anode region is

$$E_x = -2\sum_{n=\pm 1,\pm 3,}\left[\Phi_o\left(\frac{x-na}{F_n(x,z)}-\frac{x-na}{G_n(x,z)}\right)+\frac{\Phi_A r_o^2}{z_A}\left(\frac{(z-z_G)(x-na)}{G_n^2(x,z)}\right)\right], \quad \text{(C4a)}$$

$$E_z = -\sum_{n=\pm 1,\pm 3,}\left[2\Phi_o\left(\frac{z+z_G}{F_n(x,z)}-\frac{z-z_G}{G_n(x,z)}\right)-\frac{\Phi_A r_o^2}{z_A}\left(\frac{(x-na)^2-(z-z_G)^2}{G_n^2(x,z)}\right)\right]-\frac{\Phi_A}{z_A}. \quad \text{(C4b)}$$

The axial electric field at the surface of the cathode in the absence of space charge is

$$E_z(x, z=0) = -\Phi_A / z_A - \mu(x)(\Phi_G / z_G - \Phi_A / z_A), \quad \text{(C5)}$$

where the dipole term has been neglected and

$$\mu(x) = \left(\frac{2}{\ln(2 z_G / r_o) + M_o}\right)\sum_{n=\pm 1,\pm 3,}\frac{z_G^2}{(x-na)^2 + z_G^2} < 1, \quad \text{(C6)}$$

is a shielding parameter. The grid wires partially shield the electric fields associated with the anode potentials. The electron current is turned off when the grid potential is sufficiently negative so that $E_z > 0$ on the cathode, that is, no current flows when

$$\Phi_G < -\left(\frac{1-\mu}{\mu}\right)\frac{z_G}{z_A}\Phi_A. \quad \text{(C7)}$$

b) Grid Emittance Estimate

The emittance growth due to the grid can be estimated by calculating the rms angular deflection of the electrons as they propagate from the cathode, through the grid region, to the anode (see Fig. 7). The rms normalized emittance (x-direction) is $\varepsilon_{n,x} = \gamma\beta_z\left(\left\langle x^2\right\rangle\left\langle (x')^2\right\rangle - \left\langle x\,x'\right\rangle^2\right)^{1/2}$, where $\langle\ \rangle$ denotes an average over particles, $\gamma \approx 1$ is the relativistic factor, $\beta_z = \mathrm{v}_z/c$, v_z is the axial beam velocity and $x' = \partial x/\partial z$. The normalized emittance is given by $\varepsilon_{n,x} \approx \gamma\beta_z R_b\left\langle\Delta\theta\right\rangle$, where R_b is the rms beam radius, $\left\langle\Delta\theta\right\rangle = \left\langle \mathrm{v}_x/\mathrm{v}_z\right\rangle$ is the rms deflection angle. The normalized grid emittance can therefore be written as $\varepsilon_{n,x} \approx R_b\left\langle \mathrm{v}_x/c\right\rangle$. In the absence of self fields the electron deflection velocity in the x-direction is given by $\partial \mathrm{v}_x/\partial z = (q/m)E_x/\mathrm{v}_z$ where the transverse electric field near the z-axis, $|x| < a$, can be approximated by $E_x \approx -x\,\partial E_z/\partial z$, where E_x and E_z are the electric fields components associated with the dc bias and rf fields.

The transverse deflection velocity at $z = 2z_G$ is approximately given by

$$\mathrm{v}_x \approx -\frac{q}{m}\int_0^{2z_G}\frac{x}{\mathrm{v}_z}\frac{\partial E_z}{\partial z}dz \approx -\frac{q\,x}{m\left\langle \mathrm{v}_z\right\rangle}\Delta E_z, \qquad \text{(C8)}$$

where $\Delta E_z = E_z(x, 2z_G) - E_z(x, 0)$. It is assumed that the transverse electron position changed little from its initial position and $\left\langle \mathrm{v}_z\right\rangle$ is to be evaluated at $z = 2z_G$. Beyond $z \sim 2z_G$ the transverse velocity is approximately constant. For $r_a << a,\ z_G$, the effect of the dipole field part of the potential on the average electron deflection can be neglected.

To obtain an estimate for the emittance we consider a single wire centered at $z = z_G$ and $x = 0$, making use of the potential and fields given by Eqs.(C1) and (C2). The axial field difference, using Eq.(C2), is

$$\Delta E_z \approx \frac{4}{3}\mu_1(x)\left(\frac{\Phi_G}{z_G} - \frac{\Phi_A}{z_A}\right), \qquad \text{(C9)}$$

where

$$\mu_1(x) = \left(\frac{2}{\ln(2\,z_G / r_o)}\right)\frac{z_G^2}{(x^2 + z_G^2)}, \tag{C10}$$

is the shielding parameter associated with a single grid wire. The normalized transverse velocity at $z = 2\,z_G$ is

$$\beta_x \approx -\frac{4}{3}\frac{q\,x}{m\,c^2\langle\beta_z\rangle}\mu_1(x)\left(\frac{\Phi_G}{z_G} - \frac{\Phi_A}{z_A}\right). \tag{C11}$$

The maximum deflection angle occurs when $x \approx \pm a$, and the axial velocity is $\langle\beta_z\rangle \approx (2q\Phi(x,z)/mc^2)^{1/2}$ for $\langle\Delta\theta\rangle << 1$, where $\Phi(x, 2z_G) \approx 2(z_G / z_A)\Phi_A$. The grid emittance is therefore given by

$$\varepsilon_{n,grid} \approx R_b\langle\beta_x\rangle \approx \frac{2\mu_1(a)}{3}\left(\frac{a}{z_G}\right)R_b\frac{\left|\overline{\Phi}_G - (z_G / z_A)\overline{\Phi}_A\right|}{(z_G / z_A)^{1/2}\,\overline{\Phi}_A^{1/2}}, \tag{C12}$$

where $\overline{\Phi}_G = |q|\Phi_G/(mc^2)$ and $\overline{\Phi}_A = |q|\Phi_A/(mc^2)$. The electric field on the cathode for a single grid wire is $E_z(x,0) = -\Phi_A / z_A - \mu_1(x)(\Phi_G / z_G - \Phi_A / z_A)$. Using typical values for the parameters, we find that $\langle\beta_z\rangle \sim 2\times10^{-2}$ and the normalized emittance due to the grid is $\varepsilon_{n,grid} \sim 5-15\,\text{mm}-\text{mrad}$.

A number of approximations were employed in obtaining the grid emittance. More accurate estimates for the grid emittance, which include self field effects, are obtained using the PIC code TurboWAVE and are presented in Sec. III.

Appendix D: PARMELA Simulations of an IOT Gun

IOT guns have a number of characteristics necessary for use as injectors for high-power FELs, e.g., high average currents, short bunch lengths, long life times, robustness, etc. However, because the applications for which IOT guns were designed did not require low emittance, the transverse bunch emittance is typically too large for use as a high average power FEL injector. In this Appendix, we use the PARMELA code to simulate the complicated geometry and field structures of a typical IOT gun and characterize the emitted electron bunches. We show that through the use of fundamental and third harmonic rf frequencies, the bunch length is sufficiently short and the average current sufficiently high for use as a high-power FEL injector. While the resulting

emittance is large (~25 mm-mrad), it should be possible to modify the present gun design to lower the emittance, for example, by improving the anode design, using emittance compensating coils, and using a shadow grid at the cathode.

The geometry used for the PARMELA [35] simulations is shown in Figs. 14 and 15. To preserve the azimuthal symmetry of the simulation, the grid (Fig. 15) is modeled as a series of thin, concentric rings separated by a distance of 0.4 mm. For the purpose of computing the rf field, this grid is attached to a curved backing plate that confines the rf field within the grid-cathode region. In an actual gun, this backing plate is replaced by a number of radial spokes that serve to contain the rf field. In the simulations, the backing plate is transparent to electrons. A shadow grid is used to prevent electron emission directly under the wires.

The grid is biased to - 450 V dc relative to the cathode, and an rf field at the frequency of the fundamental (700 MHz) and the third harmonic is injected radially into the cathode-grid gap. The fundamental rf field has an amplitude of 9.4 kV/cm, while the anode is maintained at a potential of 35 kV. The temporal profile of the total rf field is illustrated schematically in Fig. 5. The total longitudinal field at the cathode surface is illustrated in Fig. 16.

To simulate emission at the cathode, a long, low-velocity (0.1 eV) bunch is initialized behind the cathode surface to serve as a reservoir of charge. The bunch is spatially uniform over the cross-section 0.4 cm < r < 0.9 cm, and no particles are contained in those radii corresponding to the locations of the shadow grid wires. As a particle in this bunch crosses the cathode surface, it is emitted only if it lies within the range of rf phase indicated in Fig. 5, and emission occurs over the cathode region indicated in Fig. 16. Particles that are turned around at the cathode surface are absorbed, and do not contribute to the computation. The emitted electrons are propagated by the external and space charge fields, and image charges at the cathode surface are included.

Figure 17 is a series of plots showing the evolution of the electron bunch as it starts from the cathode and travels a distance of 5 cm to the end of the gun. In this example, 46 psec (rms) bunches having a charge of 1.0 nC are generated. The average current is $\langle I_b \rangle = 0.7\,\mathrm{A}$. The transverse phase space at the location of the anode, as shown in Fig. 18a, corresponds to a projected emittance of $\varepsilon_n = 25\,\mathrm{mm-mrad}$, while the

slice emittance is ~ 26 mm-mrad. The longitudinal phase space is shown in Fig. 18b, and is characterized by a longitudinal emittance of $\varepsilon_z = 26\,\mathrm{keV}\text{-psec}$.

This simulation illustrates that it is possible to obtain from a conventional IOT gun the high average currents and short bunch lengths necessary for use as an injector for a high-power FEL. Through improved anode design and the use of emittance compensation, it is possible a similar design may produce transverse emittances of < 15 mm-mrad, as required.

References

[1] G.R. Neil, C.L. Bohn, S.V. Benson, G. Biallas, D. Douglas, H.F. Dylla, R. Evans, J. Fugitt, A. Grippo, J. Gubeli, R. Hill, K. Jordan, G.A. Krafft, R. Li, L. Merminga, P. Piot, J. Preble, M. Shinn, T. Siggins, R. Walker and B. Yunn, "Sustained kilowatt lasing in a free-electron laser with same-cell energy recovery," Phys. Rev. Lett., **84**, pp. 662-665, Jan. 2000.

[2] "Free Electron Laser High Brightness, High Average Current Injector" Report to the NAVY HEL Program Office (PMS-405) & Office of Naval Research," P. O'Shea, Panel Chairman, 28 October 2002.

[3] A. Todd, Nucl. Instrum. Methods Phys. Res. A **557**, 36 (2006).

[4] I. Ben-Zvi and I.V. Bazarov, Nucl. Instrum. Methods Research A **557**, 337 (2006).

[5] W.B. Colson, J. Blau and R.L. Armstead, Nucl. Instrum. Methods Phys. Res. A **507**, 48 (2003).

[6] D.C. Nguyen and H.P. Freund, "Possibility of a high-power, high-gain FEL amplifier," Nucl. Instrum. Methods Phys. Res. A **507**, 120, (2003).

[7] P. Sprangle, B. Hafizi and J.R. Penano, "Design of a Compact, Optically Guided,

Pinched, Megawatt Class Free-Electron Laser," IEEE J. Quantum Electron.

40, 1739-1743 (2004).

[8] I. Ben-Zvi, D. Kayran and V. Litvinenko, "High average power optical FEL amplifiers," in Proc. Int. FEL Conf., Stanford, CA 2005, p. 232.

[9] P. Sprangle, J. Penano, B. Hafizi and I. Ben-Zvi, IEEE J. Quantum Electron, **46**, pp 1135-1144 (2010).

[10] D.C. Nguyen, *et al.*, "Overview of the 100 mA average-current RF photoinjector," Nucl. Instrum. Methods Phys. Res. A, **528**, 71 (2004).

[11] S. Benson, *et al.*, "High power lasing in the IR upgrade FEL at Jefferson Lab," Proceedings of the 2004 FEL Conference, 229-232 (2004).

[12] K.L. Jensen, N.A. Moody, D.W. Feldman, *et al.*, J. Appl. Phys. **102**, 074902 (2007).

[13] C. Hernandez-Garcia, T. Siggins, S. Benson, D. Bullard, H. F. Dylla, K. Jordan, C. Murray, G. R. Neil, M. Shinn, and R. Walker, Proceedings of 2005 Particle Accelerator Conference, Knoxville, Tennessee, p. 3117; C. Hernandez-Garcia, P.G. O'Shea and M.L. Stutzman, Physics Today **61**, 44, Feb. (2008).

[14] A. Yeremian, J. Adamski, R. Kennedy, *et al.*, Proceedings of the Particle Accelerator Conference, 1989. Accelerator Science and Technology, Chicago, IL, USA, pp. 657-659.

[15] R. Koontz *et al.*, IEEE Trans. Nuclear Sci. **NS-28**, 2213 (1981).

[16] T.I. Smith, "The Stanford Superconducting Linear Accelerator," *Physics of Quantum Electronics*, Vol. 8, ed. S.F. Jacobs, et al. [Addison-Wesley, Reading, MA, 1982], pp. 77–87.

[17] V. P. Bolotin *et al.*, "Status of the Novosibirsk Terahertz FEL," in Proc. 2004 FEL Conf., pp. 226–228

[18] K. Togawa, T. Shintake, T. Inagaki, *et al.*, Phs. Rev. ST Accel. Beams, **10**, 020703 (2007)

[19] T. Shintake, *et al.*, Phys. Rev. ST Accel. Beams **12**, 070701 (2009).

[20] A.S. Gilmore, *Principles of Travelling Wave Tubes*, Artech House, Boston, MA

1994.

[21] P. Frigola, G. Andonian, S. Reiche, *et al.*, Proceedings of the Particle Accelerator Conference, 1993. Accelerator Science and Technology, Portland, OR, USA.

[22] M. Reiser, *Theory and Design of Charged Particle Beams*, Wiley, New York, NY 1994.

[23] T. Wangler, *RF Linear Accelerators*, Wiley, New York, NY 1998.

[24] R.C. Davidson, *Physics of Nonneutral Plasmas*, Addison-Wesley, Redwood, CA, 1990.

[25] R. Vaughan, IEEE Trans. Elec. Dev. ED-**33**, 1925 (1986).

[26] S. H. Gold and G. S. Nusinovich, Rev. Sci. Instrum. **68**, 3945 (1997).

[27] Y.Y. Lau, Y. Liu and R.K. Parker, Phys. Plasmas 1, 2082 (1994).

[28] J.D. Jarvis, *et al.*, "Development of diamond field-emitter arrays for free-electron lasers," in Proc. Int. FEL Conf., Gyeongju, Korea, p. 232 (2008).

[29] J.D. Lawson, The *Physics of Charged-Particle Beams*, Oxford, University Press, Oxford, UK 1988.

[30] D.F. Gordon, W.B. Mori, and T.M. Antonsen, Jr., "A Ponderomotive Guiding Center Particle-in-Cell Code for Efficient Modeling of Laser Plasma Interactions," IEEE Trans. Plasma Sci. **28**, 1224-1232 (2000); D.F. Gordon, "Improved Ponderomotive Guiding Center Algorithm," IEEE Trans. Plasma Sci. **35**, 1486-1488 (2007).

[31] C.W. Roberson and P. Sprangle, "A Review of Free-Electron Lasers," Phys. Fluids B, vol. **1**, pp. 3-42, Jan. 1989.

[32] C. Beard, Nucl. Instrum. Methods Phys. Res. A **557**, 276 (2006).

[33] D. H. Priest and M. B. Shrader, Proc. IEEE **70**, 1318 (1982).

[34] E. G. Zaidman and M. A. Kodis, IEEE Trans. Electron Devices **38**, 2221 (1991).

[35] J. H. Billen, *PARMELA Documentation*, Los Alamos Report LA-UR-96-1835, Revised December 2005.

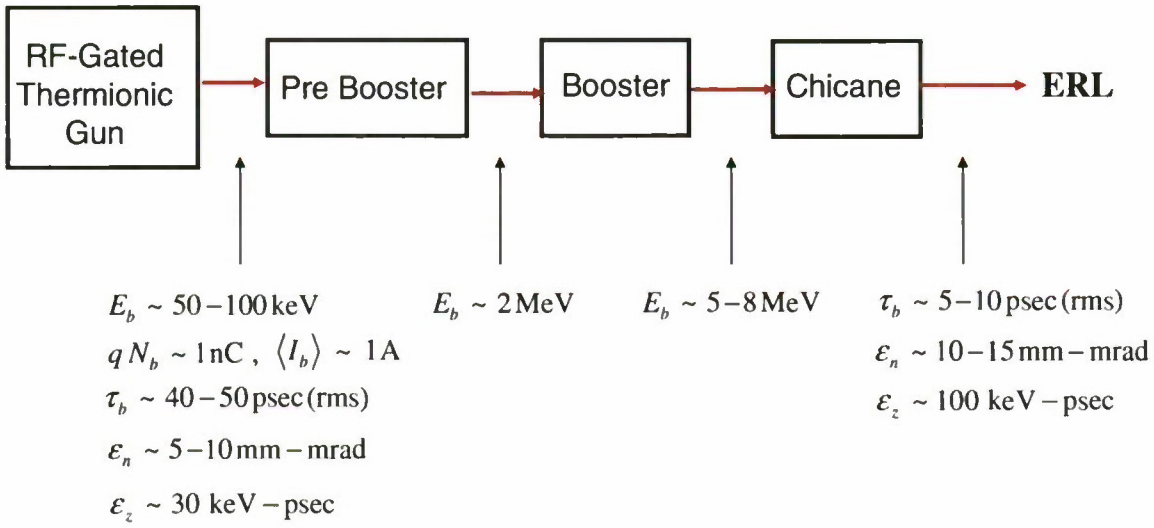

Figure 1: Schematic of injector for an FEL employing an energy recovery linac (ERL). The source of electrons is an rf-gated, gridded thermionic gun. Electrons are accelerated in booster cavities and bunched in a magnetic chicane before entering the ERL. Typical electron beam parameters associated with the stages are indicated in the figure.

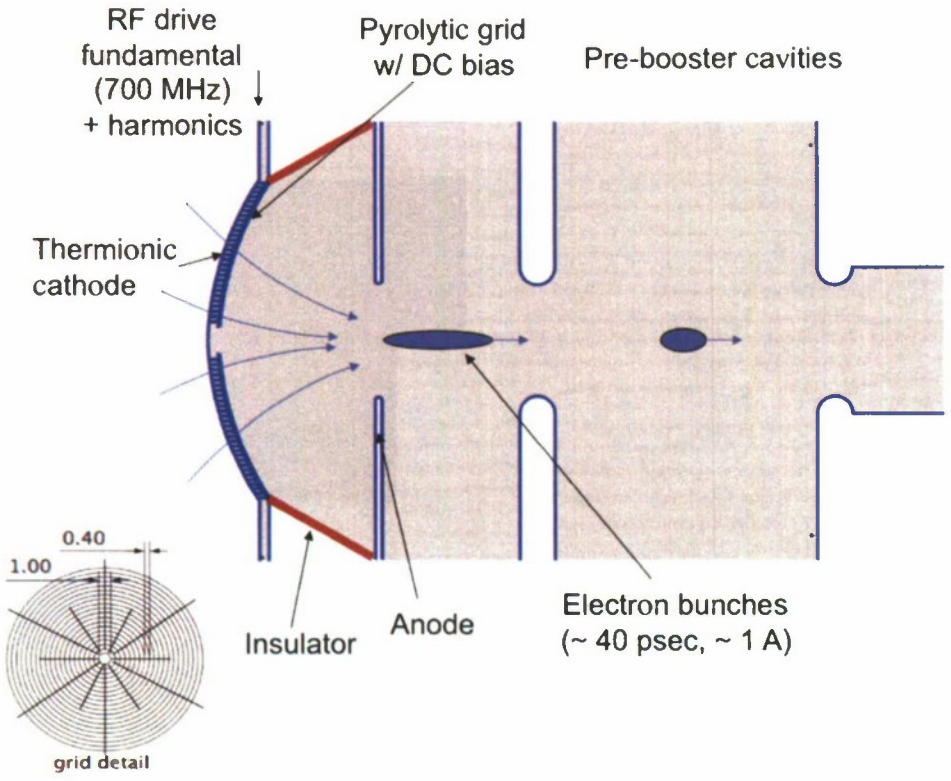

Figure 2: Schematic diagram of rf-gated thermionic gun for high-average current FEL operation. The rf-gated, gridded thermionic gun consists of a dispenser or single-crystal CeB_6 cathode and pyrolytic graphite grid. The grid consists of a series of concentric rings and is biased negatively and driven positive by the rf relative to the cathode. Typical grid dimensions are indicated in the figure in mm. The potential on the grid is modulated at the fundamental (~700MHz) and 3rd harmonic (2.1 GHz) of the linac frequency to produce short (~ 40 psec rms), high-charge (~1 nC) electron bunches. The rf field of the fundamental loads every bucket in the linac with an electron bunch. The electron energy exiting the pre booster is ~ 2 MeV. The grid voltage is negative and typically in the range of 100 - 300 V.

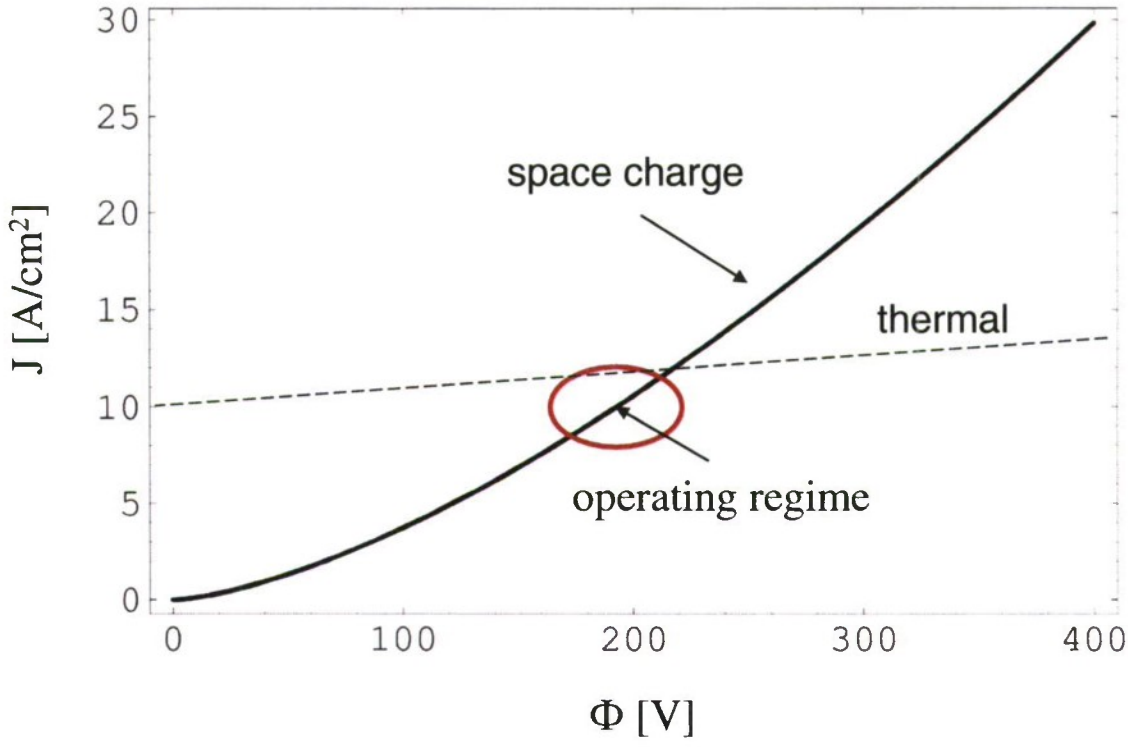

Figure 3: Current density-voltage characteristics, J vs Φ. The solid curve is the space charge limit (Child-Langmuir) and the dashed curve is the thermal limit (Richardson-Dushman-Schottky). The characteristics are for the case with gap spacing $d = 250\,\mu\text{m}$, work function $\Phi_{WF} = 1.9\,\text{eV}$ and cathode temperature $T_c = 1300\,\text{K}$. The optimum operating region is near the intersection of the two limits where the current density is not a sensitive function of the cathode temperature.

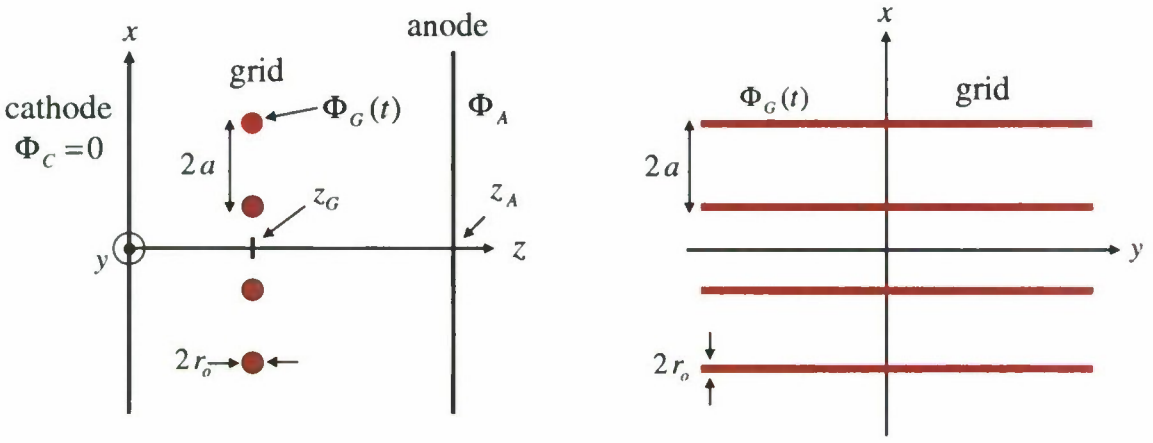

Figure 4: Schematic of grid wires used for obtaining an estimate of the beam emittance due to the grid. The rings comprising the grid in Fig. 2 are modeled by an array of parallel grid wires. The grid wires, with radius r_o, are at a potential Φ_G, are parallel to the y-axis, separated by a distance $2a$ and located at $z = z_G$.

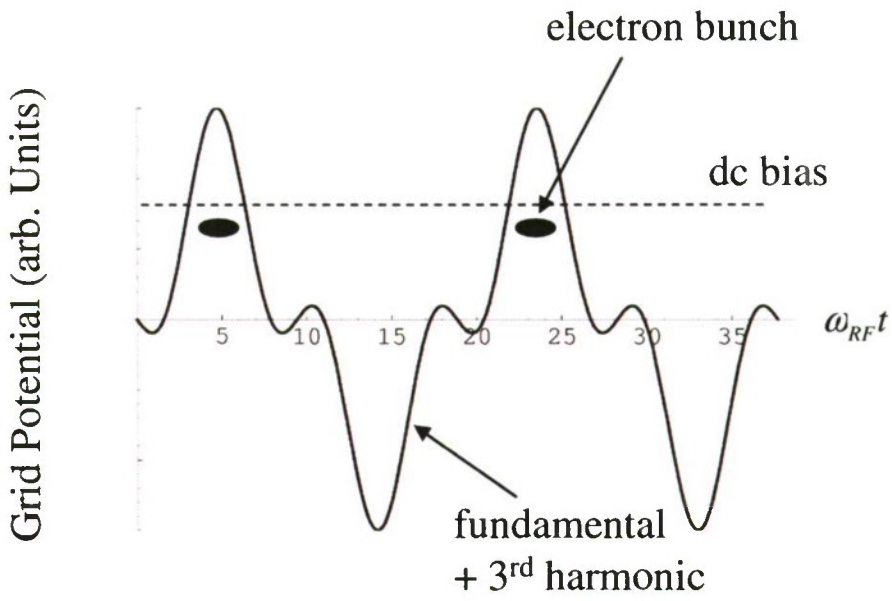

Figure 5: Waveform consisting of the fundamental and third harmonic (blue curve). The amplitude of the third harmonic is taken to be half that of the fundamental. The DC bias (dashed line) limits the electron bunch length to ~ 90° of the third harmonic, while filling every bucket.

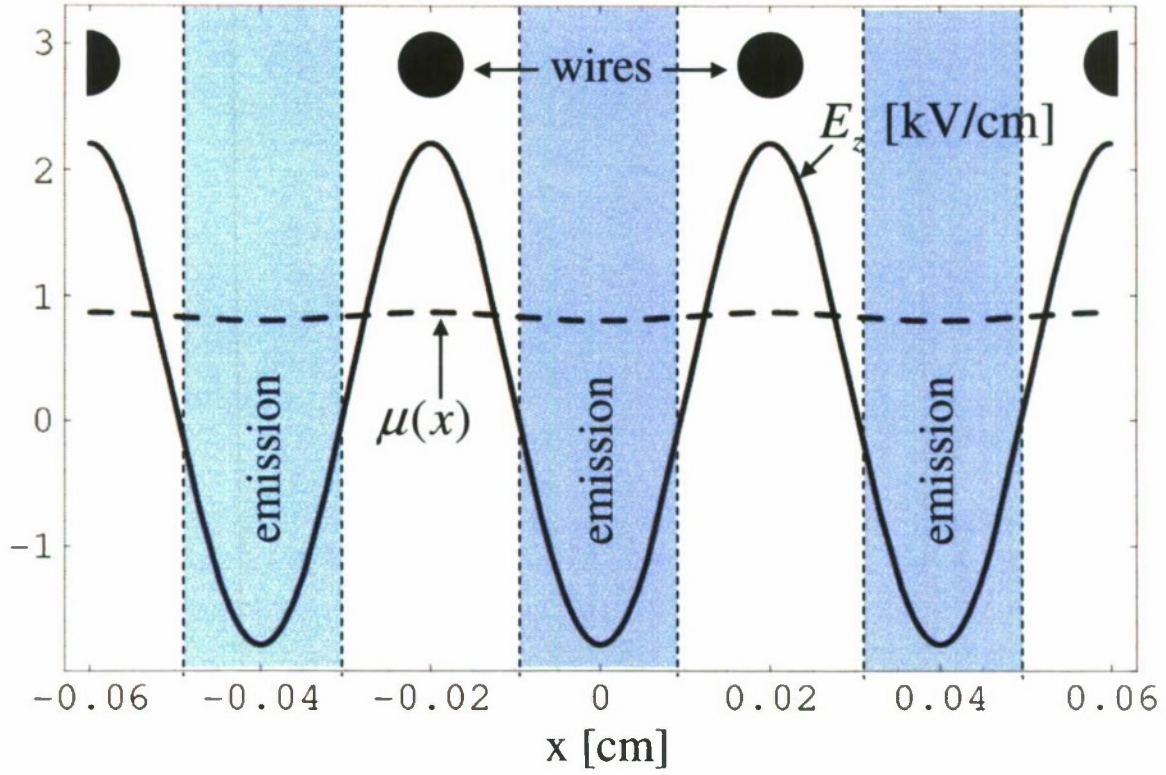

Figure 6: Plot of shielding parameter $\mu(x)$ and the electric field on the cathode, $E_z(x, z=0) = -\Phi_A / z_A - \mu(x)(\Phi_G / z_G - \Phi_A / z_A)$, versus transverse position for the configuration in Fig. 4. The grid is at a distance $z_G = 250\,\mu\text{m}$ from the cathode and the grid potential is $\Phi_G(t) = -360 - 38\cos(\omega_{RF} t) + 36\cos(2\omega_{RF} t) - 33\cos(3\omega_{RF} t)$ in units of volts where the fundamental frequency is $f_{RF} = \omega_{RF} / 2\pi = 700\,\text{MHz}$ and the plot is for $t = \pi / \omega_{RF}$. The cathode-anode gap is $z_A = 1\,\text{cm}$, the cathode-anode potential is 50 kV and the grid wire radius is $r_o = 30\,\mu\text{m}$. The shielding parameter, in the absence of space charge, is $\mu = 0.8$ between the wires and $\mu = 0.87$ beneath the wires. It should be noted that the electron flux from the cathode is a sensitive function of $\mu(x)$. Electron emission from the cathode is transversely limited to the regions near the minima of $\mu(x)$.

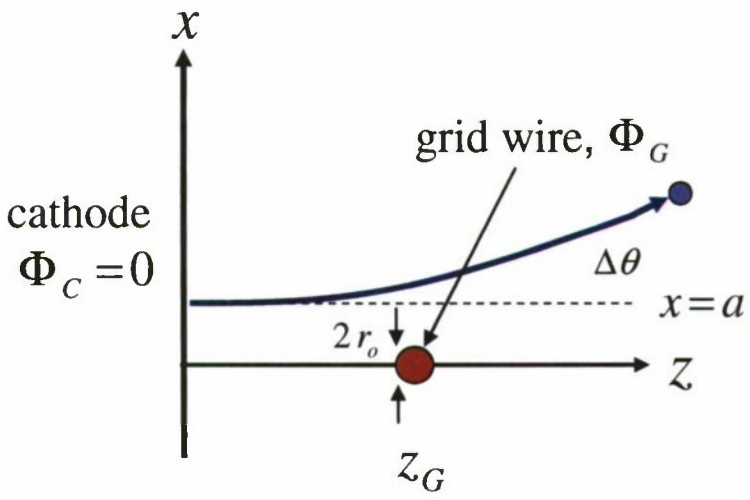

Figure 7: Calculation of emittance due to a single grid wire. Here the cathode is at ground potential and located at $z=0$, the grid wire is at potential Φ_G, located at $z=z_G$ and has radius r_o. An electron with impact parameter a is deflected through an angle $\Delta\theta$ due to grid wire.

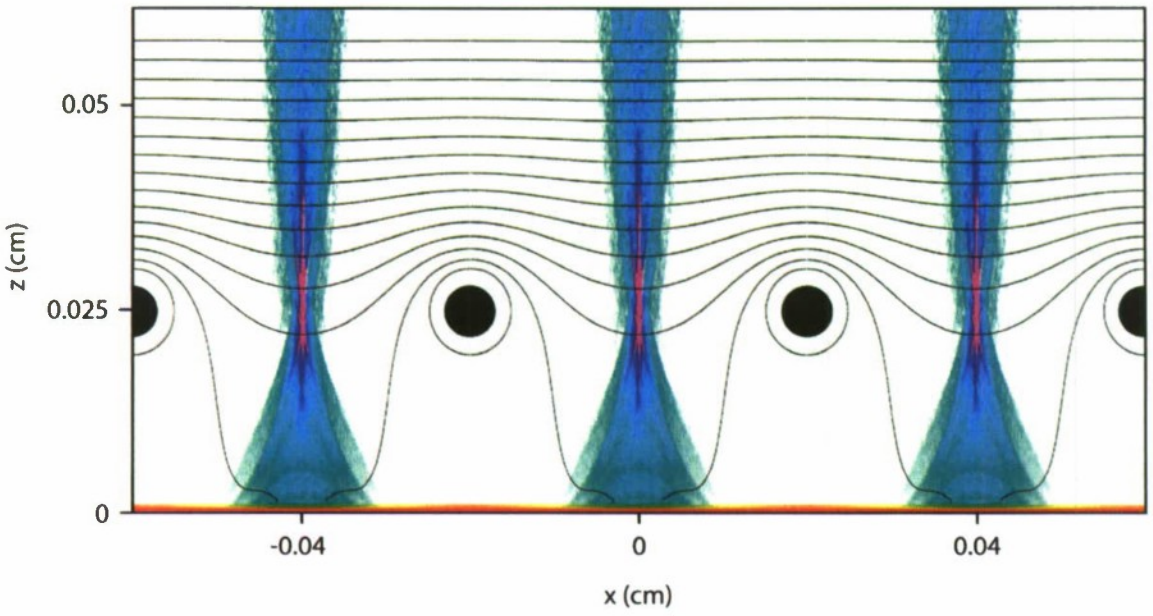

Figure 8: TurboWAVE simulations of current density in cathode-grid region including the effects of space charge. The color scale indicated current density, with red more dense and blue less dense. The cross sections of four grid wires are shown. The cathode is located at $z=0$, the lower boundary of the figure. Parameters are the same as in Fig. 6. Black curves show the equipotentials.

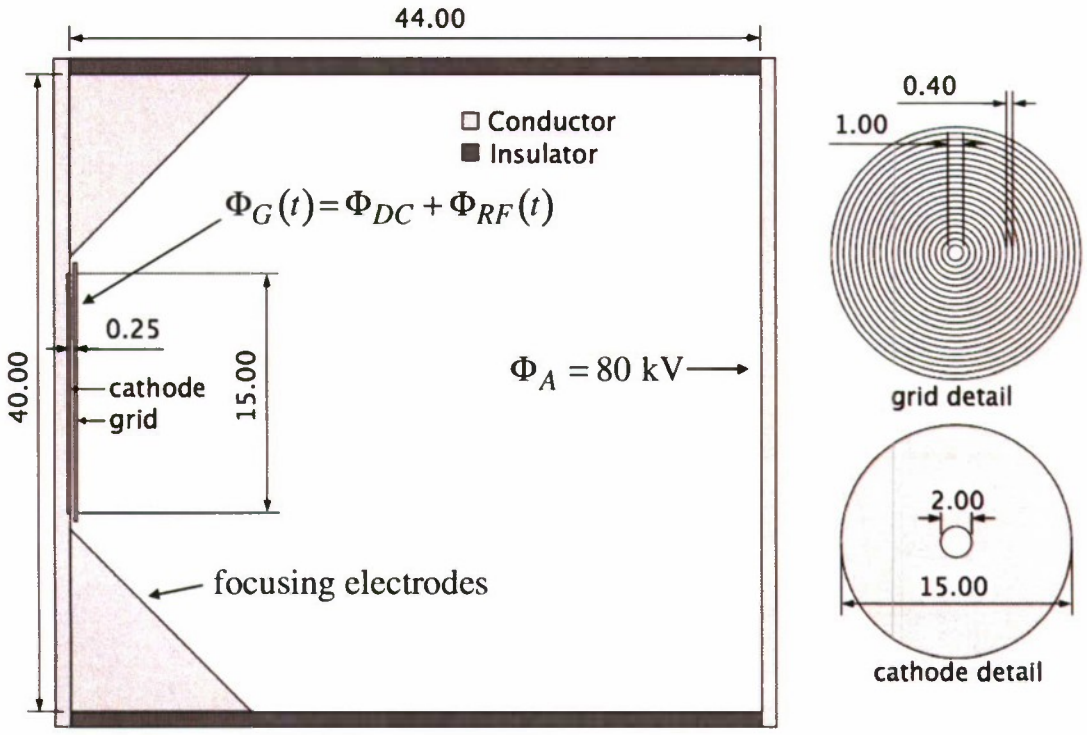

Figure 9: Gun geometry for TurboWAVE PIC simulations. The closed box on the left is bounded by insulators on the top and the bottom, the cathode on the left and anode on the right. The 45 degree focusing electrodes are also shown. The cathode is grounded, the anode is at 80 kV and the grid potential consists of a DC contribution Φ_{DC}, and a time-varing RF contribution $\Phi_{RF}(t)$. The cross section of the cathode and the grid are shown on the right. All dimensions are in mm.

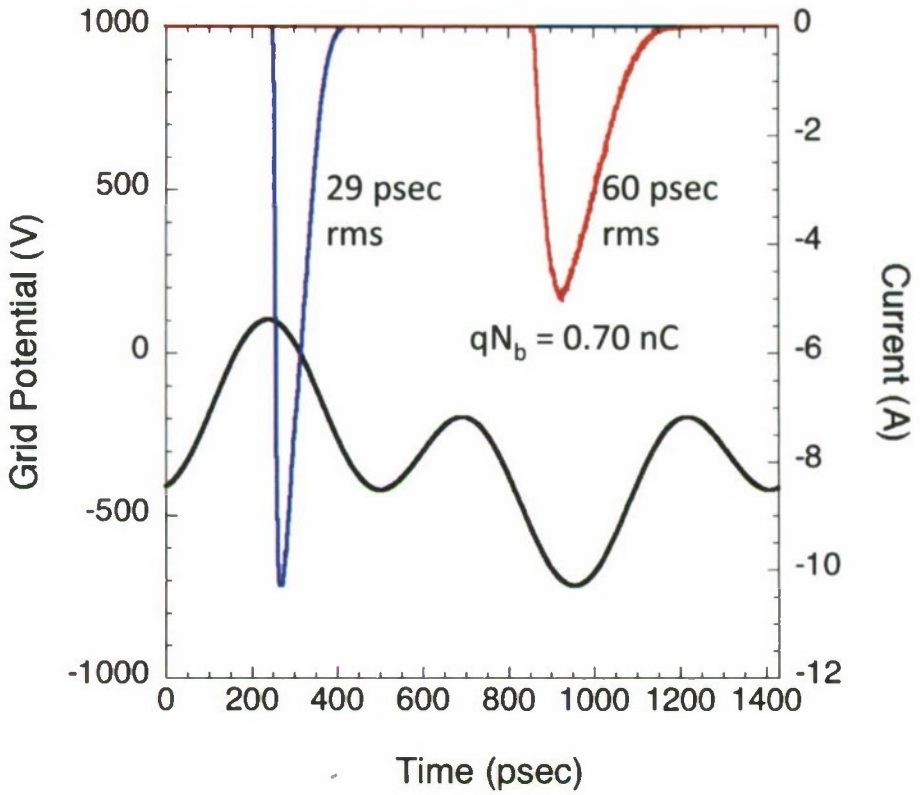

Figure 10: TurboWAVE simulations of current pulses at the grid and at the anode for the geometry shown in Fig. 9. The current pulses produced at the grid plane and the anode plane are shown in blue and red, respectively, while the time varying potential on the grid wires consisting of a DC and RF contributions is shown in black. A bunch with a 60 psec (rms) duration and 0.7 nC of charge crosses the anode resulting in an average current of $\langle I_b \rangle = 0.5\,\mathrm{A}$.

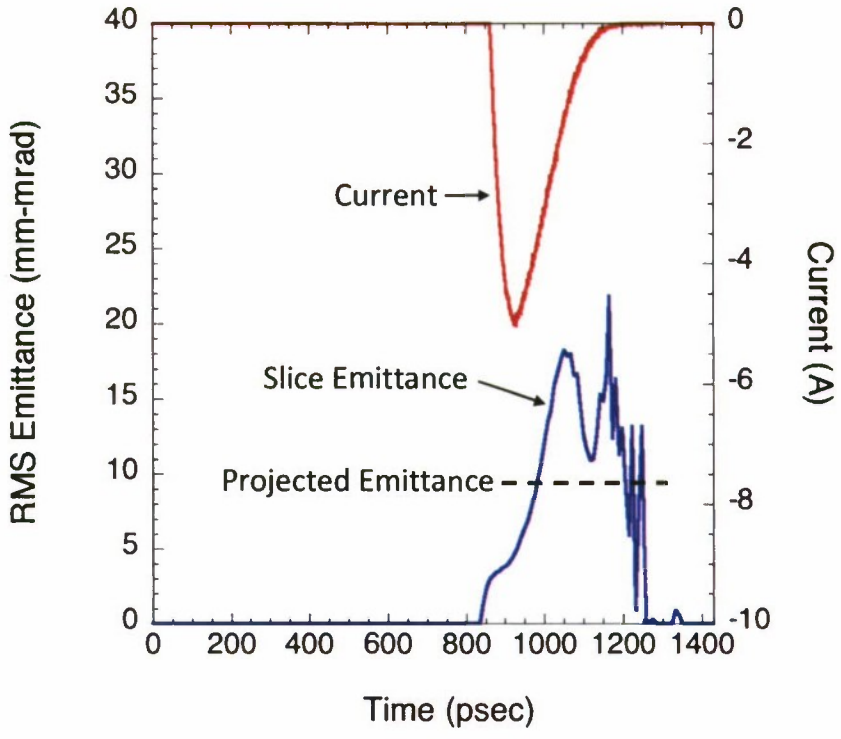

Figure 11: Simulated current and emittance at the anode for the geometry shown in Fig. 9. The red curve shows the current and the blue curve shows the slice emittance. The slice emittance at the peak of the current pulse is $\varepsilon_n \sim 5\,\mathrm{mm-mrad}$. The projected emittance $\varepsilon_n = 8.9\,\mathrm{mm-mrad}$ is shown by the dashed horizontal line.

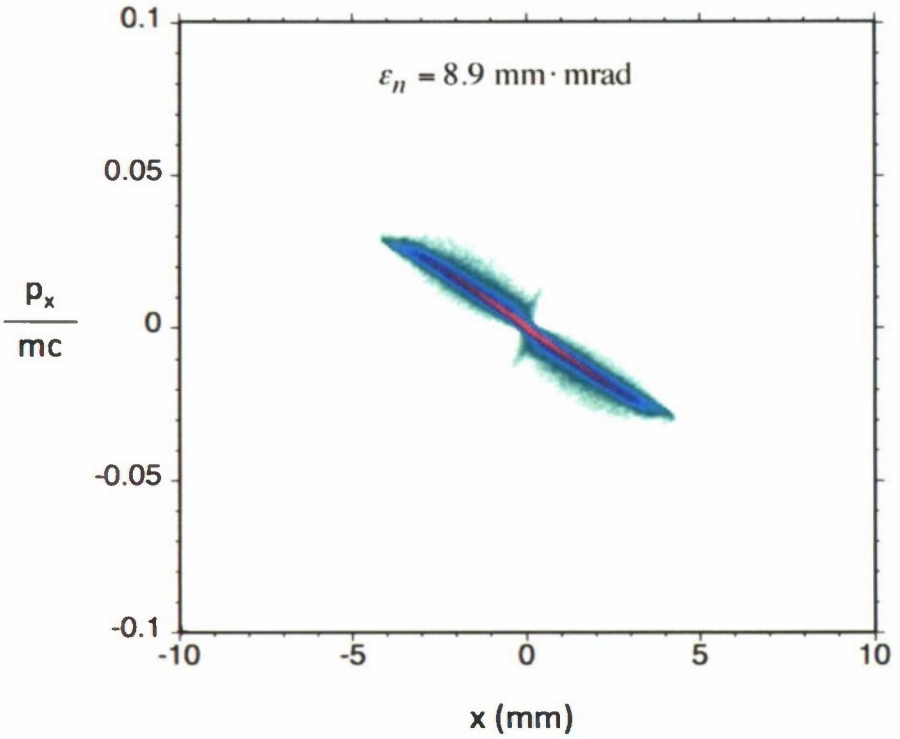

Figure 12: Projected transverse phase space for the gun geometry of Fig. 9. The ordinate is x component of the momentum normalized to mc and the abscissa is the x coordinate. The projected normalized emittance is $\varepsilon_n = 8.9$ mm-mrad.

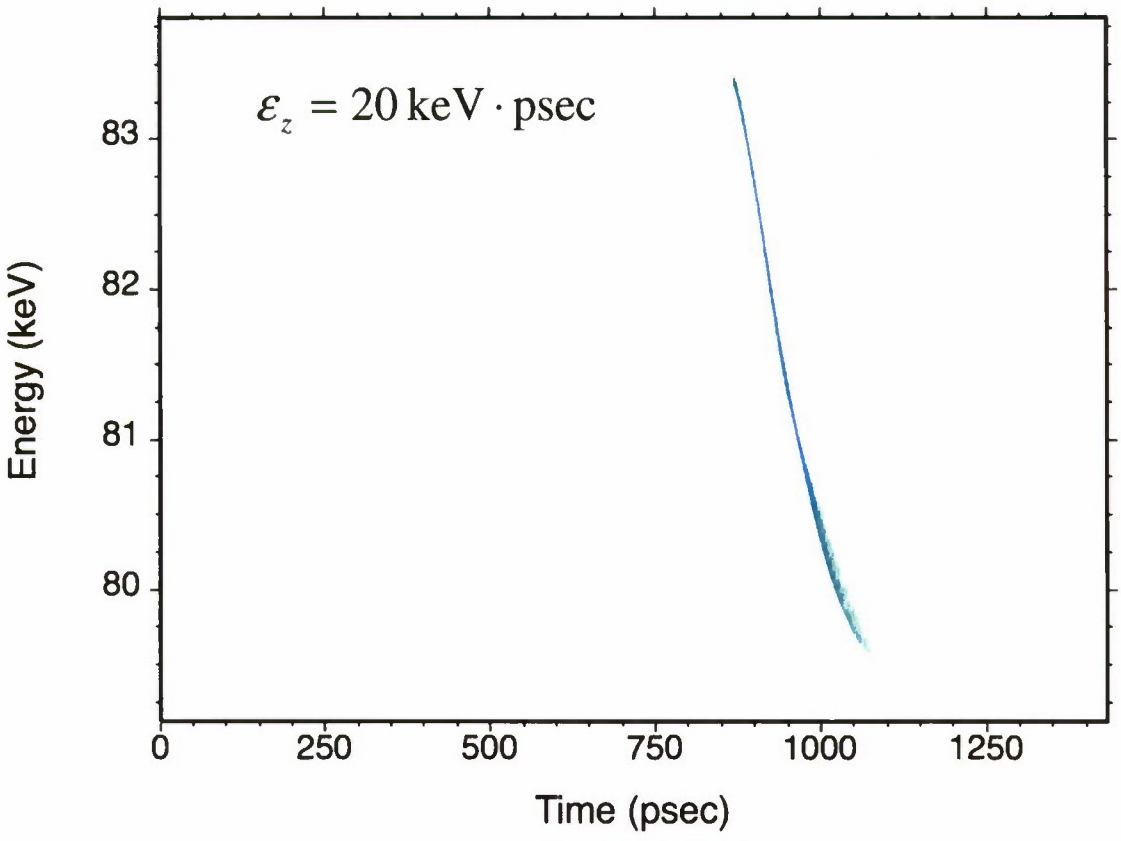

Figure 13: Longitudinal phase space (energy vs time) for the gun geometry of Fig. 9. The normalized longitudinal emittance is $\varepsilon_z = 20$ keV - psec.

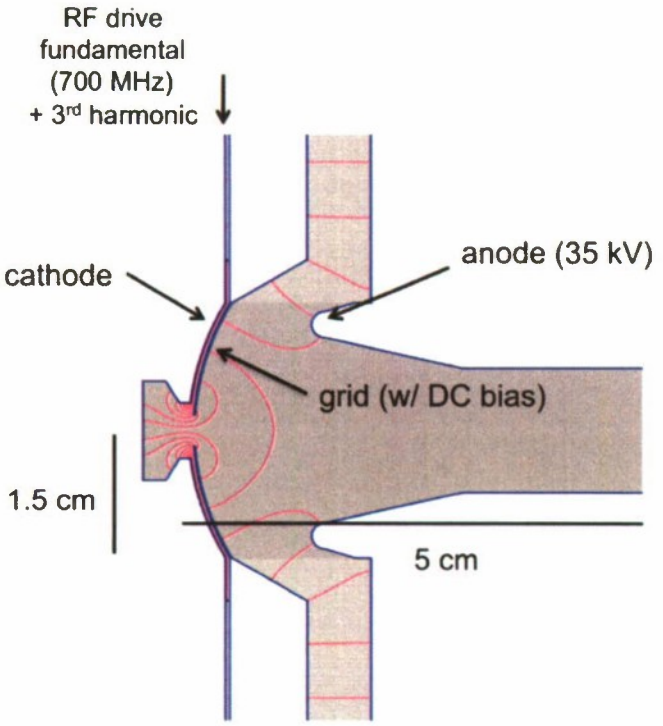

Figure 14: Geometry of a thermionic IOT gun used for the PARMELA simulations of Fig. 17. The cathode-grid gap is 0.25 mm. Fields driven at the fundamental (700 MHz) and third harmonic are injected into the cathode-grid region, and the grid has a bias of -450V. The RF fields were computed using SUPERFISH, while the DC fields were computed using POISSON. Field lines of the fundamental (700 MHz) field are shown. The time-dependent potential at the location of the grid peaks at 160 V.

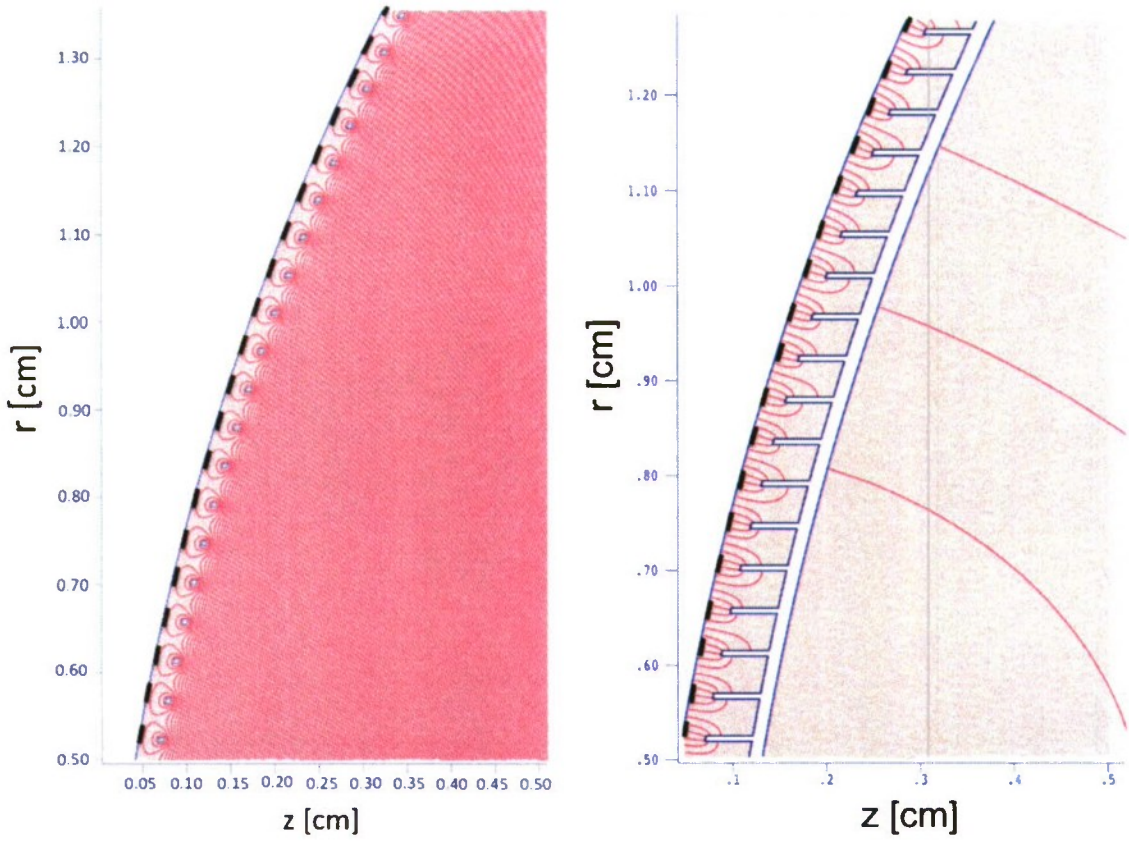

Figure 15: Close-up of the grid region used in the PARMELA simulations of Fig. 17. Black lines illustrate the shadow grid used to prevent emission from the cathode beneath the grid wires. (Left) For the purpose of computing the static field, the grid is modeled as a series of concentric rings of radius $r_o = 30\mu m$. Curves denote contours of the electric potential due to the bias voltages on the anode and the grid. (Right) For the purpose of computing the rf field, the grid is modeled as a series of thin, concentric rings attached to a curved backing plate which confines the rf field to the grid-cathode region. The backing plate is transparent to electrons in the simulations. Curves denote field lines of the fundamental (700 MHz) rf field.

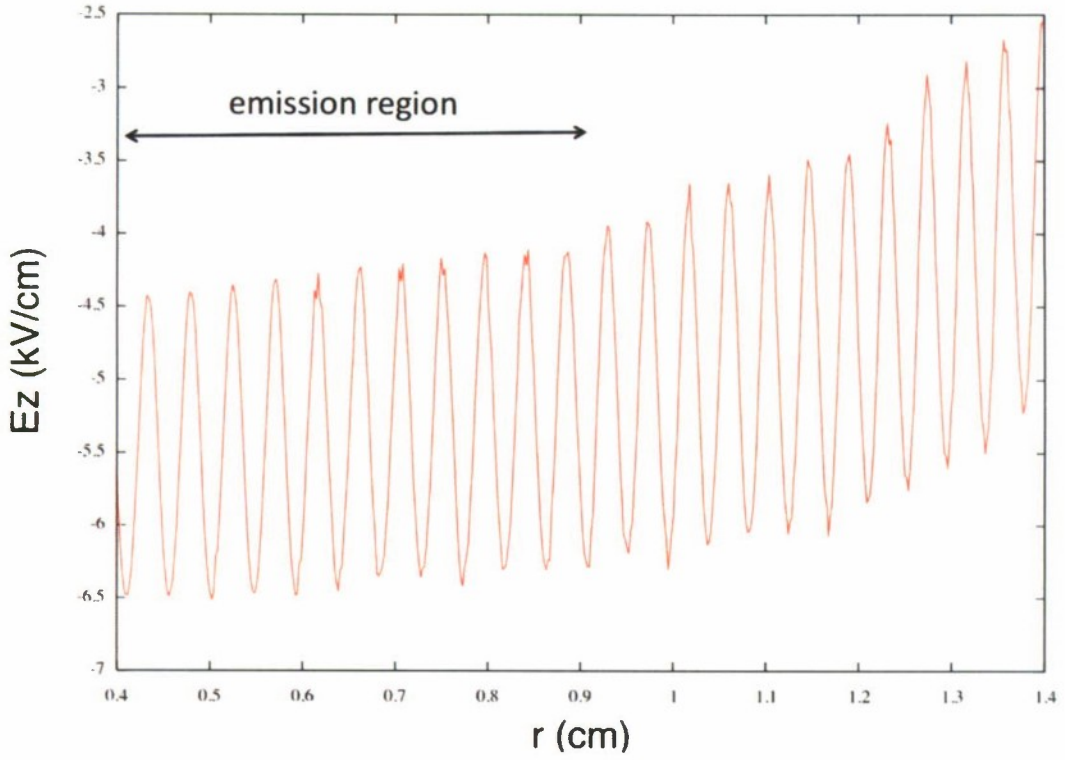

Figure 16: Electric field at the cathode used for PARMELA simulations. The total electric field across the cathode surface is plotted versus radial distance from the symmetry axis. At a given point on the cathode, the field takes the form $E_z = E_{z,DC} + E_{z,1}\sin(\omega_{RF}t) + E_{z,3}\sin(3\omega_{RF}t)$, where $E_{z,DC} \approx 11$ kV/cm, $E_{z,1} \approx -9.4$ kV/cm, and $E_{z,3} \approx 9$ kV/cm. The field is illustrated for $t = \pi/2\omega_{RF}$, at the peak of emission. Emission occurs only at those radii within the indicated region.

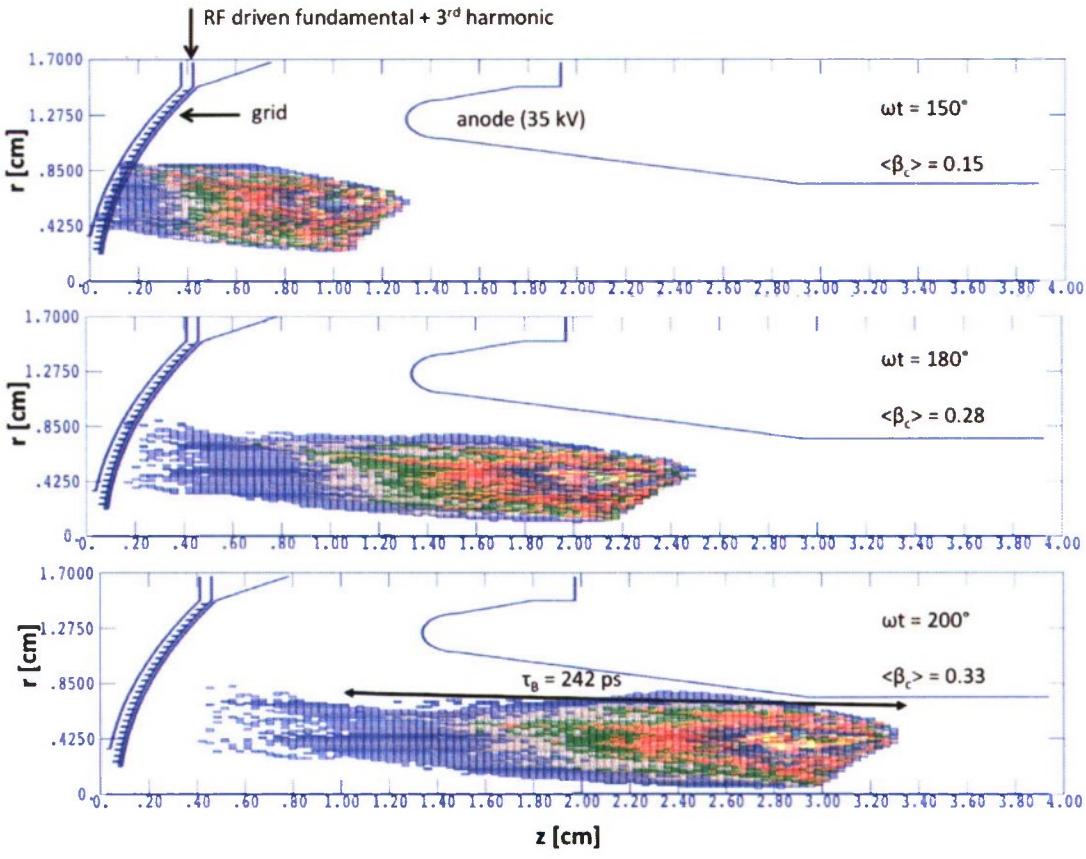

Figure 17: PARMELA simulation of an rf-gated, gridded thermionic gun. The plots show the generation of an electron bunch with end-to-end duration of 242 psec and a normalized emittance of 25 mm-mrad. The grid is biased to - 450 V dc, and the anode is biased to 35 kV relative to the cathode. The amplitude of the rf field in the cathode-grid gap is 9.4 kV/cm. The time and corresponding value of the normalized centroid velocity, β_C, is indicated in the figures.

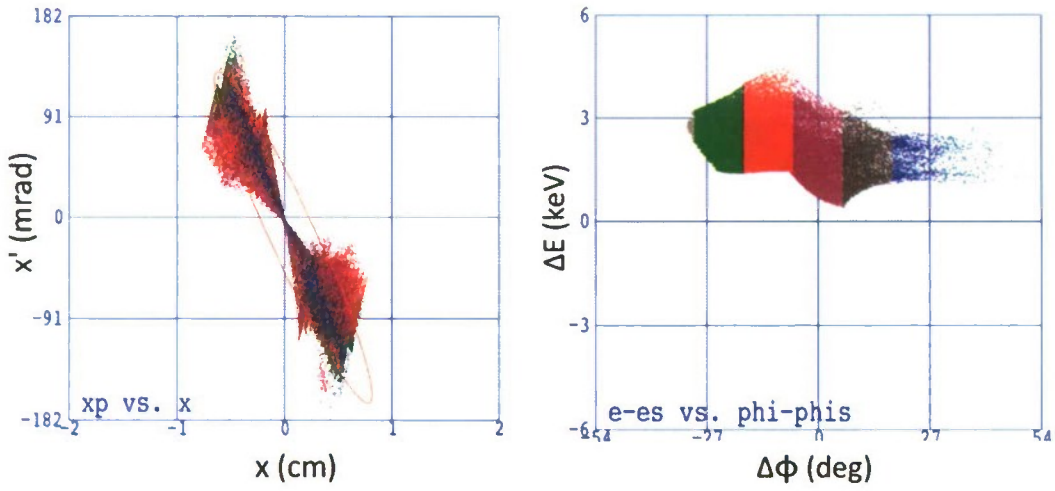

Figure 18: (a) Transverse and (b) longitudinal phase space from the PARMELA simulation of Fig. 17 at the location of the anode (z = 1.5 cm). The normalized transverse emittance is 28 mm-mrad and the longitudinal emittance is 26 keV-psec. Particles are grouped by color into six longitudinal slices, with each slice containing particles of a given range in rf phase at $z - 1.5\,\mathrm{cm}$.

Cathode-Grid Gap, z_G	250 μm
Cathode-Anode Gap, z_A	1 - 3 cm
Grid Wire Radius, r_o	30 μm
Grid Wire Separation, 2a	400 - 500 μm
Cathode Radius, R_c	0.5 – 1.5 cm
Cathode-Grid Voltage, Φ_G	100 - 300 V
Cathode-Anode Voltage, Φ_A	30 - 50 kV
RF Grid Modulation Freq., f_{RF}	500 MHz – 2.5 GHz
Cathode Current Density, J	10 – 15 A/cm^2
Cathode Temperature, T_c	1200 – 1400 K
Cathode Workfunction, Φ_{WF}	1.6 – 2.1 eV
Vacuum Level	10^{-7} - 10^{-8} Torr

Table I. Typical range of parameters in an rf-gated, gridded thermionic gun in which a conventional dispenser cathode is employed.